Biomaterials 53 (2015) 86–94

Contents lists available at ScienceDirect

Biomaterials

journal homepage: www.elsevier.com/locate/biomaterials

# Spatial coordination of cell orientation directed by nanoribbon sheets

Toshinori Fujie [a, b, 1], Xuetao Shi [a, 1], Serge Ostrovidov [a], Xiaobin Liang [a], Ken Nakajima [a], Yin Chen [c], Hongkai Wu [a, c, *], Ali Khademhosseini [a, d, e, f, *]

[a] WPI-Advanced Institute for Materials Research, Tohoku University, Sendai 980-8578, Japan
[b] Department of Life Science and Medical Bioscience, Graduate School of Advanced Science and Engineering, Waseda University, Tokyo, Japan
[c] Department of Chemistry & Division of Biomedical Engineering, Hong Kong University of Science & Technology, Hong Kong, China
[d] Center for Biomedical Engineering, Department of Medicine, Brigham and Women's Hospital Harvard Medical School, Harvard-MIT Division of Health Sciences and Technology Massachusetts Institute of Technology, Cambridge, MA 02139, USA
[e] Wyss Institute for Biologically Inspired Engineering at Harvard University, Boston, MA 02115, USA
[f] Department of Physics, King Abdulaziz University, Jeddah 21569, Saudi Arabia

ARTICLE INFO

*Article history:*
Received 24 December 2014
Accepted 2 February 2015
Available online 9 March 2015

*Keywords:*
Nanoribbon sheet
Micropattern
Bilayer
Cell orientation
Cell assembling
Myoblasts

ABSTRACT

Spatial coordination of cell orientation is of central importance in tissue/organ construction. In this study, we developed microfabricated poly(lactic-co-glycolic acid) (PLGA) nanoribbon sheets with unique structures, using spin-coating and micropatterning techniques, in order to generate a hierarchically assembled cellular structure consisting of murine skeletal myoblasts (C2C12). The nanoribbon sheets were composed of aligned PLGA nanoribbons in the center, and strips on four sides which take a role as bridges to connect and immobilize the aligned nanoribbons. Such unique structures facilitated the alignment of C2C12 cells into bilayer cell sheets, and cellular alignment was directed by the aligned direction of nanoribbons. The nanoribbon sheets also facilitated the construction of multilayer cell sheets with anisotropic (orthogonal) and isotropic (parallel) orientations. The enhanced expression of myogenic genes of C2C12 cells on the bilayer cell sheets demonstrated that the nanoribbons induced C2C12 cell differentiation into mature myoblasts. The micropatterned nanoribbon sheets may be a useful tool for directing cellular organization with defined alignment for regenerative medicine and drug screening applications.



## 1. Introduction

Recapitulation of hierarchical assembly of cells and extracellular matrix (ECM) is of great significance to engineer functional tissues. The exquisite microscale and nanoscale architectures of tissues induce various cell behaviors, including alterations in cell adhesion, morphology, orientation, and various intracellular signaling pathways [1–3]. For example, cardiac and skeletal muscles possess striated structures consisting of sarcomeres packed into highly organized bundles. Skeletal muscle fibers are organized as parallel bundles, whereas cardiac muscle fibers are arranged at branching angles [4,5]. To engineer an artificial niche or scaffold that simulates the natural topographic landscape of tissues (e.g. muscles), one potential approach is to construct micro-organized cellular structures. Efforts are underway to engineer multilayer cell-material composites using various techniques, including laser-guided directed writing, micro-molding of cell-laden hydrogels, and dielectrophoretic force-cell micropatterning [6–8]. However, these techniques have been limited by complicated process requirements and a lack of suitable biological properties. For example, alginate hydrogels have been widely used to develop microparticles and microfibers; however, anchorage-dependent cells poorly proliferate on these substrates.

Micropatterning, which facilitates the generation of simple or complicated motifs (e.g. grooves, pillars, and wells) on various surfaces with flat or curved features, is a powerful tool for directing cell behaviors, including spatial arrangement and differentiation [9–11]. However, despite the significant efforts, the construction of a three-dimensional (3D) structure with a well-defined cell arrangement using micropatterning remains a challenge [12]. To address this challenge, we aimed to develop a technique that

* Corresponding authors. WPI-Advanced Institute for Materials Research, Tohoku University, Sendai 980-8578, Japan.
*E-mail addresses:* chhkwu@ust.hk (H. Wu), alik@rics.bwh.harvard.edu (A. Khademhosseini).
[1] These authors contributed equally to this work.

http://dx.doi.org/10.1016/j.biomaterials.2015.02.028
0142-9612/

combines the superior qualities of micropatterning to build multilayered cellular constructs.

Advances in nanotechnology have led to the development of freestanding, ultrathin polymeric films (referred to as "nanosheets"). Nanosheets, which are composed of biodegradable and biocompatible materials (e.g. polylactic acid and polysaccharides), have unique features, such as strong adhesion to dry or hydrated surfaces, high flexibility (allowing adherence to flat or curved surfaces), and excellent transparency [13–17]. Here, we aimed to utilize these properties to develop engineered matrices for constructing multilayer micropatterned cell sheets. To this end, it was important for the nanosheets to display excellent biodegradability and cell adhesion as well as low cytotoxicity to facilitate cell residence and the regulation of cell orientation [18]. Poly(lactic-co-glycolic acid) (PLGA) is a copolymer approved by the Food and Drug Administration (FDA) for use in a number of therapeutic devices [19,20]. The tunable degradation (regulated by the composition of lactic and glycolic acids) and safety of PLGA (commercial products include Bone-Fix and drug-releasing microspheres) have been confirmed [21].

In this study, we developed microfabricated PLGA nanoribbon sheets with a unique structure using spin-coating and micropatterning techniques to generate a hierarchically assembled cellular structure consisting of aligned murine skeletal myoblasts (C2C12). This material bridges the gap between the well-developed two-dimensional (2D) micropatterning for cell patterning and the 3D construction of multicellular structures. We anticipate that the nanoribbons may be a useful tissue engineering tool for directing cellular organization with defined alignment and microstructure, which could be useful for engineering 3D tissue structures for applications in regenerative medicine and drug screening. For example, freestanding aligned cell sheets could serve as a multilayered cardiac patch, artificial skin, or engineered skeletal muscle.

## 2. Materials and methods

### 2.1. Materials

PLGA (70/30; MW: 97,000) was purchased from Polysciences Inc. (PA, US). Dichloromethane and PVA (MW: 13,000–23,000) were purchased from Kanto Chemical Inc. (Tokyo, Japan). Alexa Fluor 594-conjugated phalloidin and 4′6-diamidino-2-phenylindole dihydrochloride (DAPI) were pursued from Sigma–Aldrich (US). A mouse monoclonal anti-fast skeletal myosin antibody and an Alexa Fluor 488-conjugated goat anti-mouse antibody (ab-7784) were purchased from Abcam (US) and Invitrogen (US), respectively. All cell culture-related reagents were obtained from Invitrogen. Petri dishes (60 mm Ø) were purchased from Orange Scientific (Belgium).

### 2.2. Fabrication and characterization of freestanding PLGA nanoribbon sheets

PLGA nanoribbon sheets were developed by a combination of micropatterning and spin-coating techniques. First, PLGA nanoribbon sheets were generated by spin-coating 5 mg/mL PLGA-dichloromethane solution (4000 rpm, 40 s) on a micro-grooved polydimethylsiloxane (PDMS) replica (2 × 2 $cm^2$), and baked on a hot plate (80 °C, 90 s). Then, a thin PVA layer (10 wt%, 300 μL) was cast onto the PDMS replica, which was dried in a desiccator overnight in order to remove the residual water in the PVA layer. After being dried, the PLGA/PVA bilayer was carefully detached from the PDMS replica using tweezers. Next, freestanding PLGA nanoribbon sheets were obtained by soaking the PLGA/PVA bilayer film in a water-filled Petri dish in order to dissolve the PVA layer. Then, the rinsing water was completely removed and the dish was dried in a desiccator overnight, allowing for the physical adhesion of the freestanding PLGA nanoribbon sheet onto the dish surface. Subsequently, the dish was filled with water and left for 2 days for the complete removal of residual PVA. Prior to the cell seeding, the nanoribbon sheet-coated dish was sterilized under the UV lamp for 1 h. In case of disordered PLGA nanoribbons, the flat edge part of the PLGA/PVA bilayer film was cut by scissors and gently released in water. Additional rising steps were the same as the process described above.

### 2.3. Morphology and surface properties of the nanosheets

The thickness of PLGA nanoribbon sheets was analyzed by a surface profiler (Dektak150, Veeco Instruments Inc., Plainview, NY). The morphology of the PLGA nanoribbon sheets was observed using a field emission scanning electron microscope (FE-SEM; JIB-4600F).

### 2.4. Fabrication of bilayer cell sheets

PLGA nanoribbon sheets (1 cm × 1 cm) were physically adhered on a Petri dish, and thirty thousand C2C12 murine skeletal myoblasts (American Type Culture Collection (ATCC), US) were seeded. After 7 days of culture, the myoblasts exhibited approximately 80% confluence. The first cell layer was then coated with a 50 μg/mL fibronectin solution to promote anchoring the cells of the second layer to those in the first layer. After 30 min of incubation, the first cell layer was covered with another PLGA nanoribbon sheets, which was then seeded with sixty thousand C2C12 myoblasts. The bilayer cell sheets were placed in an incubator for 5 h to facilitate cell adhesion. Additionally, 500 μL of culture medium was added to compensate for the consumption of medium. Next, 10 mL of cell culture media (DMEM, 10% FBS, and 1% penicillin/streptomycin) was added and the cells were cultured for another 5 days.

### 2.5. Cell viability and morphology

The Viability/Cytotoxicity Kit (Invitrogen) was used to determine cell viability. The calcein AM and ethidium homodimer-1 in the kit stain live and dead cells green and red, respectively. Thirty thousand cells were seeded on a single-layer (1 cm × 1 cm) PLGA nanoribbon sheet. After 3 days of culture, the cells on the single-layer nanoribbon sheets were washed with PBS and incubated in 2 mL of PBS for 15 min at 37 °C. The cells were washed with PBS 3 times, and imaged using a fluorescence microscope (Zeiss, Germany).

### 2.6. Quantification of myoblast alignment

After 3 days of culture, the cells on the single-layer nanoribbon sheets were washed with PBS, and then fixed and permeabilized using 4% (w/v) formaldehyde for 15 min followed by 0.1% (v/v) Triton X-100 for 5 min. The cells were stained with phalloidin-conjugated Alexa-Fluor 594 (Invitrogen, USA) and DAPI (Sigma–Aldrich, USA) to visualize F-actin and cell nuclei, respectively. The F-actin (in red color) and cell nuclei (in blue color) were then imaged using fluorescence microscopy (Zeiss, Germany). Cellular alignment was quantitatively evaluated based on the alignment angle, which was defined as the angle between the long axis of a nucleus considered as elliptical and the groove direction (200 nuclei were analyzed using ImageJ software package). Alignment angles were then categorized in 10° increments. Cells with alignment angles less than 10° were considered aligned.

### 2.7. Cell staining using CellTracker

To visualize the cell organization on the bilayer cell sheets, we used CellTracker to distinguish the cells in two layers. C2C12 myoblasts were cultured on the first layer of the PLGA nanoribbon sheet, and then stained using CellTracker™ Green dye (Invitrogen) after 7 days of culture. Briefly, CellTracker™ Green dye was dissolved in anhydrous dimethylsulfoxide (DMSO) to a concentration of 10 mM and then diluted to 5 μM in serum-free medium. The prepared working solution was added to the cell layer for 30 min at 37 °C. The working solution of dye was then replaced with fresh medium, and the cell layer was incubated for an additional 30 min at 37 °C. The cell layer was then washed with PBS and cultured in culture medium overnight. Subsequently, the second cell layer was constructed on the surface of the first layer with fibronectin treatment. The cells in the second layer were stained with CellTracker™ Orange dye before seeding on the microgrooved nanosheets. Briefly, when C2C12 cells cultured in a flask (170 $cm^2$) reached confluence, 12 mL of a working solution of CellTracker™ Orange dye (5 μM in serum-free medium) was added to the flask and incubated for 30 min at 37 °C. The dye was then replaced with fresh medium, followed by incubation for another 30 min at 37 °C. The cells cultured in the flask were then washed with PBS and cultured in culture medium overnight. The cells stained with CellTracker™ Orange dye were suspended and then seeded onto the second set of nanoribbon sheets. At 8 days of culture, a fluorescence microscope (Zeiss, Germany) was used to observe the cell orientation of the generated bilayer cell sheet.

### 2.8. Myotube formation

To induce myotube formation in the bilayer cell sheet, the cell culture medium was replaced after 8 days of culture with a differentiation medium composed of DMEM supplemented with 2% horse serum (HS), and 1% penicillin/streptomycin.

### 2.9. Immunocytochemistry

After 12 days of culture, the cell sheets with a number of generated myotubes were fixed in a 4% paraformaldehyde solution for 15 min at room temperature, then washed twice with PBS and placed into a 0.1% Triton X-100 solution for 5 min. Non-specific binding sites were blocked using 10% goat serum (Invitrogen) for 1 h at room temperature. The cells were incubated with primary antibody (mouse monoclonal anti-fast skeletal myosin antibody, 1:1000 dilution) overnight at 4 °C. The cell sheets were washed 3 times with PBS and then incubated with secondary antibody (Alexa Fluor 488-conjugated goat anti-mouse antibody, 1:1000 dilution) for 1 h at room temperature. Alexa Fluor 594-conjugated phalloidin (for F-actin staining) and DAPI (for nucleus staining) were then added to the cell sheets and incubated for 30 min at 37 °C.

### 2.10. Quantification of myotube alignment

After staining for myosin and nuclei, the cells were visualized, and myotubes were identified. The length of the myotubes (containing more than 3 nuclei) was measured using the AxioVision software. The degree of cell or myotube alignment was defined as the angle formed between the cell nucleus or a myotube and the axis of the aligned nanoribbons, such that an angle below 10° corresponded to aligned cell or myotube. More than 100 cells were analyzed in each experiment using ImageJ software [22].

### 2.11. Quantitative reverse transcription-polymerase chain reaction (qRT-PCR)

After 12 days of culture, the cells in the bilayer sheets were lysed using TRIzol reagent (Sigma–Aldrich, US). Isolated RNA was purified using an RNA purification kit (Sigma–Aldrich). The purified RNA, primers (the sequences of the primers are shown in Table S1), and SuperScript III Platinum SYBR Green (Invitrogen, US) were mixed and analyzed on a MyiQ2 two-color RT-PCR detection system (Bio-Rad, US).

### 2.12. Statistical analysis

The data are displayed as the means ± standard deviations, and at least three replicates were conducted in each experiment. Every experiment was Student's t-test and analysis of variance (ANOVA) followed by Tukey's multiple comparison tests were performed to analyze the difference between experimental groups.

## 3. Results

### 3.1. Fabrication of nanoribbon sheets

The PDMS replicas had microgrooved channels with a spacing of 50 or 100 μm (Fig. S1), that was embossed to the PLGA layer (Fig. 1A). The PLGA layer was prepared on the PDMS replicas by spincoating. (i.e. In order to cover the PDMS replica with polymer solution uniformly, the pristine PDMS replica was sometimes spincoated by polymer-free solvent, beforehand.) A thin PVA layer prepared on the PLGA-spincoated PDMS replicas was working as a supporting layer to detach the PLGA nanoribbons without structural distortion in the PLGA layer. Then, the freestanding PLGA nanosheet with aligned nanoribbons (referred as "nanoribbon sheet") was obtained by dissolving the PVA layer in water (Fig. 1B). The resulting PLGA nanoribbon sheets were subsequently deposited on the surface of a Petri dish (to construct the first layer) or maintained in water or PBS for later use.

### 3.2. Morphology of nanoribbon sheets

The morphology of PLGA nanoribbon sheets was imaged using scanning electron microscopy (SEM). As shown in Fig. 1C, the PLGA nanoribbons showed uniform alignment with the thickness of 48 ± 7 nm. The height of each nanoribbon at the edges was greater than 4000 nm (Fig. 1D). We postulated that the PLGA nanoribbon sheets were composed of aligned canal-like nanoribbons. The strips in four sides of the nanoribbon sheets take a key role as bridges, which connected and immobilized the aligned nanoribbons. To verify this unique structure, we cut the edge of the strips of the nanoribbon sheets, resulting in the disordered nanoribbons (Fig. 2).

The cells grown on the PLGA aligned nanoribbon sheets showed excellent organization (Fig. 3), with more than 80% of the cells on the nanoribbons exhibiting an alignment parallel to the direction of the nanoribbons. The cells grew not only on the nanoribbons but also on the slots part between two aligned ribbons.

### 3.3. Fabrication of bilayer C2C12 cell sheets

To construct the bilayer cell sheets, C2C12 myoblasts were seeded on the nanoribbon sheets physically adhered to a Petri dish. After 7 days of culture, the myoblasts exhibited approximately 80% confluence (the first cell layer was generated). Before covering the first cell sheet with the second layer of nanoribbons, we coated the first cell sheet with a 50 μg/mL fibronectin solution to promote the adhesion of the second cell sheet. After incubation for 30 min, the first cell sheet was covered with the second layer of nanoribbons, followed by the addition of C2C12 myoblasts. This process generates cell–cell adhesions, which strongly anchor cells to other cells and are typical structures found in mature heart muscle [22–24]. Here, the procedure used for fibronectin coating was important for enhancing the cell–cell interactions (Fig. 4A) because myoblasts cultured *in vitro* showed weak anchorage between cells. Fibronectin, a key protein in cell adhesion, significantly promoted the interaction between the first and the second layers of the cell sheets (Fig. 4B and C). Additionally, the unique structure of the nanoribbon sheets was also beneficial for building the bilayer cell sheets because the slots between two nanoribbons enhanced the cell–cell interactions between the two layers (Figs. 4A and 5A). To identify and quantify the distribution of the cells on the different nanoribbon layers, the samples were stained with CellTracker™. The cells on the first and second layers were stained with CellTracker™ Green and Orange dyes, respectively. To avoid fluorescence quenching of CellTracker™ stained cells, cell orientation of the bilayer cell sheet was analyzed at 8 days of culture. Both of the

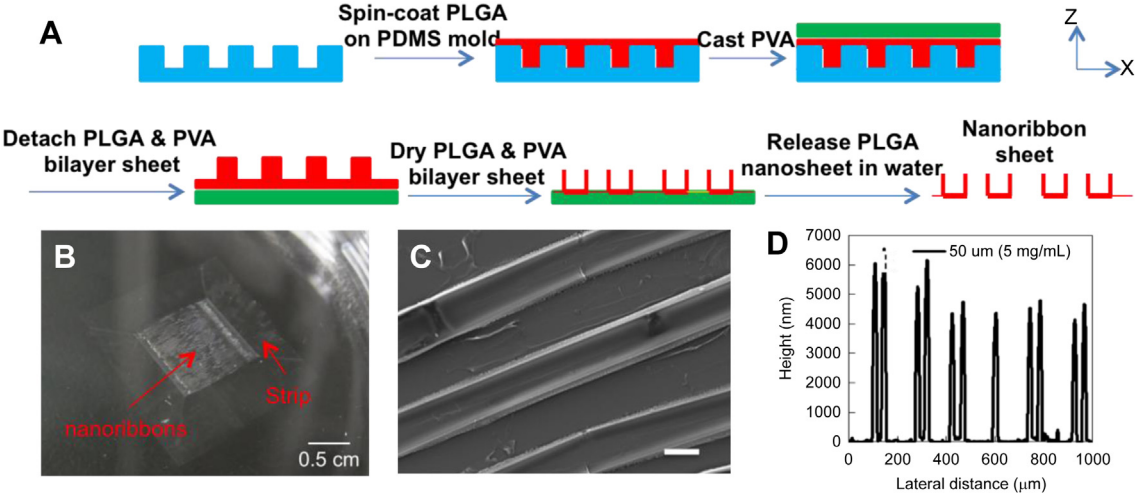


**Fig. 1.** Generation of microfabricated PLGA nanoribbon sheets. (A) Schematic of the process used for the generation of nanoribbon sheets. (B) & (C) Optical and SEM images of nanoribbon sheets with a groove spacing of 50 μm (scale bar for C: 20 μm). (D) Height of each nanoribbon with a groove spacing of 50 μm.

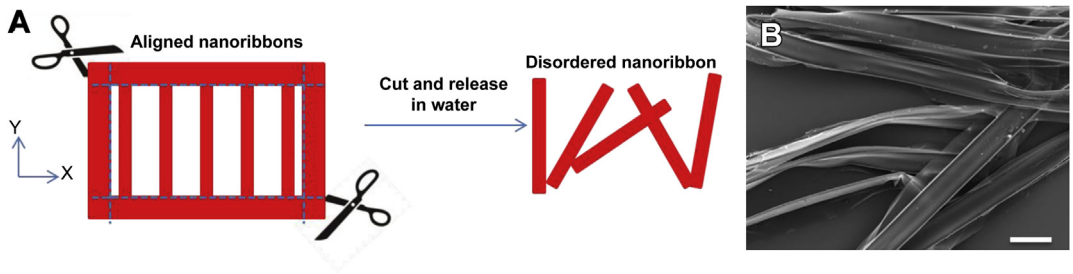


**Fig. 2.** Verification of the structure of nanoribbon sheets. (A) Schematic of the process to obtain disordered nanoribbons from the single nanoribbon sheet. (B) SEM image of disordered nanoribbons (scale bar: 50 μm).

cell layers showed significant alignment parallel to the direction of the nanoribbons (Fig. 5B). Importantly, the cells on the first layer displayed better alignment (31%) than those on the second layer (23%) (Fig. 5C). These results suggest that the longer culture period promoted the cell alignment along the direction of the nanoribbons.

### 3.4. Myotube alignment on bilayer cell sheets

Myotubes, or multi-nucleated fibers generated from the fusion of myoblasts, play a crucial role in myogenesis [25]. The alignment of myotubes, which resembles the physiological alignment of muscle fibers in skeletal muscle or cardiac tissue, is important for the contractility of these tissues [26–28]. After the generation of bilayer cell sheets, a cell differentiation medium was used to induce myotubes formation after 8 days of culture. To quantify the effect of cell alignment on the assembly of myotubes, myotubes were stained using immunofluorescence at 12 days (Fig. 6A). We investigated the formation and alignment of myotubes on a single-layer cell sheet (A-single layer), and on anisotropic (A-bilayer, orthogonal) and isotropic (I-bilayer, parallel) bilayer cell sheets (Fig. 6B and C). The myotubes on each sheet exhibited well-defined alignment. In contrast, the myotubes on the random cell sheet (R-single layer, without nanoribbons) showed a tangled arrangement (Fig. S2). The myotube alignment was approximately 25%, 37%, and 46% on the anisotropic (A-bilayer) and isotropic (I-bilayer) bilayer cell sheets and on the single-layer cell sheet (A-single layer), respectively. In contrast, only 10% of the myotubes showed alignment on the random cell sheet (R-single layer). The length of the myotubes was also measured (Fig. 6D). The average length of the myotubes on the single layer was approximately 600 μm due to the long culture duration (high cell density). The average length of the myotubes on the anisotropic and isotropic bilayer cell sheets was slightly shorter than that of the myotubes on the single-layer cell sheet, which likely occurred because the culture duration of the second layer was significantly shorter than that of the first layer (at 5 and 12 days, respectively), resulting in shorter myotubes on the second layer. The myotubes on the random bilayer cell sheets showed the shortest average length (approximately 350 μm). Overall, the myotubes on the organized cell sheets were not only highly aligned but also significantly longer than those on the random cell sheets, with approximately 40 nuclei observed in certain myotubes.

### 3.5. Construction of the myotubes generated on the bilayer cell sheets

Interestingly, we observed a significant contraction of the myotubes in the bilayer cell sheets at 12 days, even without the use of electrical stimulation (Movie S1). In contrast, the myotubes on the single-layer cell sheet did not exhibit contraction under the same cell culture conditions. This effect may have been observed because the cells on the first layer acted as a soft substrate for the contraction of the myotubes on the second layer. A soft substrate composed of organized cells facilitates the formation of functional myotubes compared with a hard substrate [29]. In this regard, we further investigated the mechanical property of the cell sheet-based substrates using an atomic force microscope (AFM). In

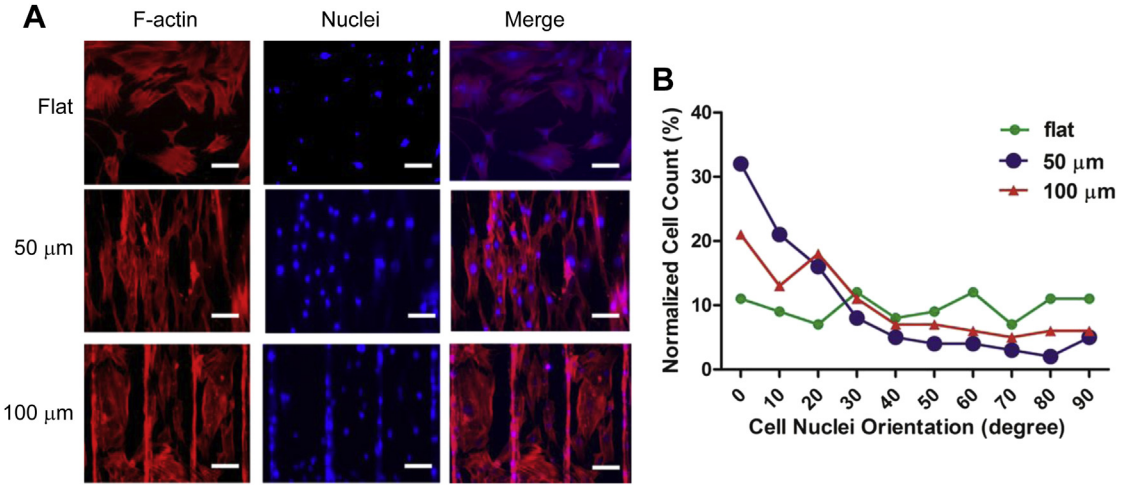


**Fig. 3.** Fluorescence images of C2C12 cells after 3 days of culture on aligned nanoribbon sheets with a groove spacing of 50 or 100 μm or on flat nanosheets. (A) F-actin and nuclear staining (scale bars: 20 μm). (B) Histogram of cell orientation on each sheet.

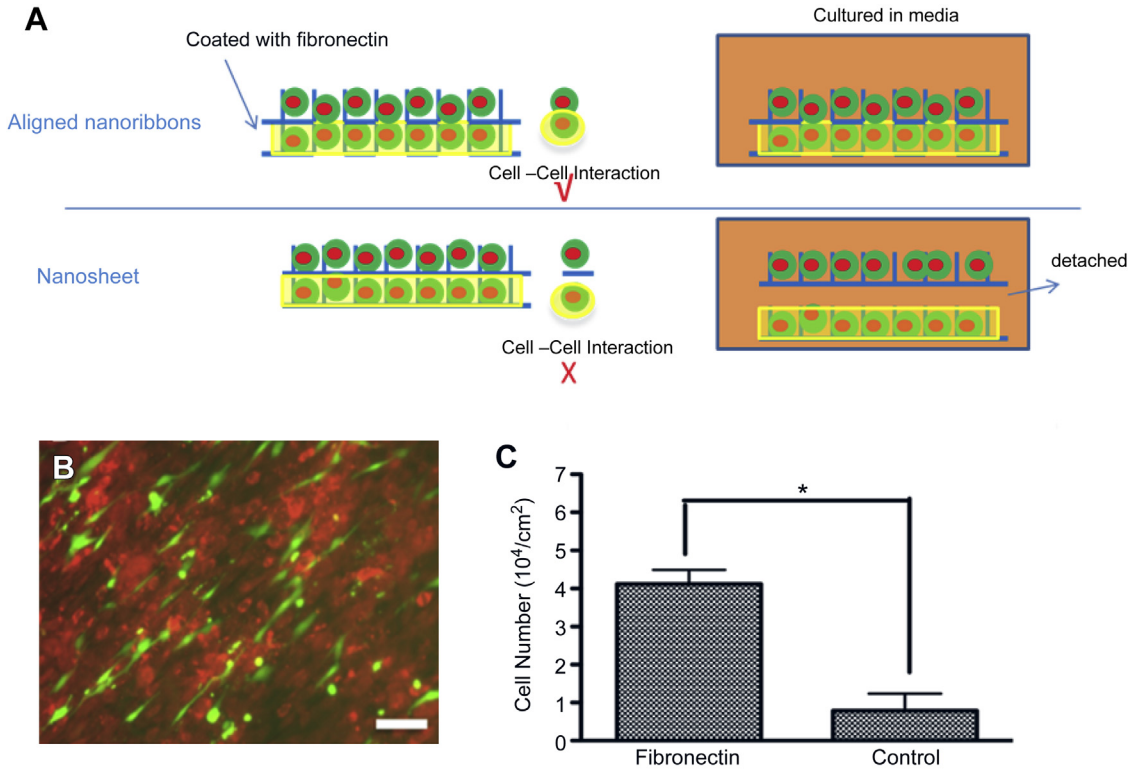


**Fig. 4.** Fibronectin treated nanoribbon sheets promoted the interaction of bilayer cell sheets. (A) Schematics of the generation of bilayer cell sheets with aligned nanoribbon sheets and of the failure to generate bilayer cell sheets with traditional grooved micropatterns that do not have slots for cell–cell interactions). (B) Fluorescence images of cells on flat or anisotropic (orthogonal) cell bilayers without fibronectin treatment. The cells on the first and second layers were stained using CellTracker Orange and Green, respectively (scale bars: 100 μm). (C) Number of cells that adhered to the first cell layer with or without (control) fibronectin treatment. *Indicates statistical significance at the 95% confidence level. (For interpretation of the references to color in this figure legend, the reader is referred to the web version of this article.)

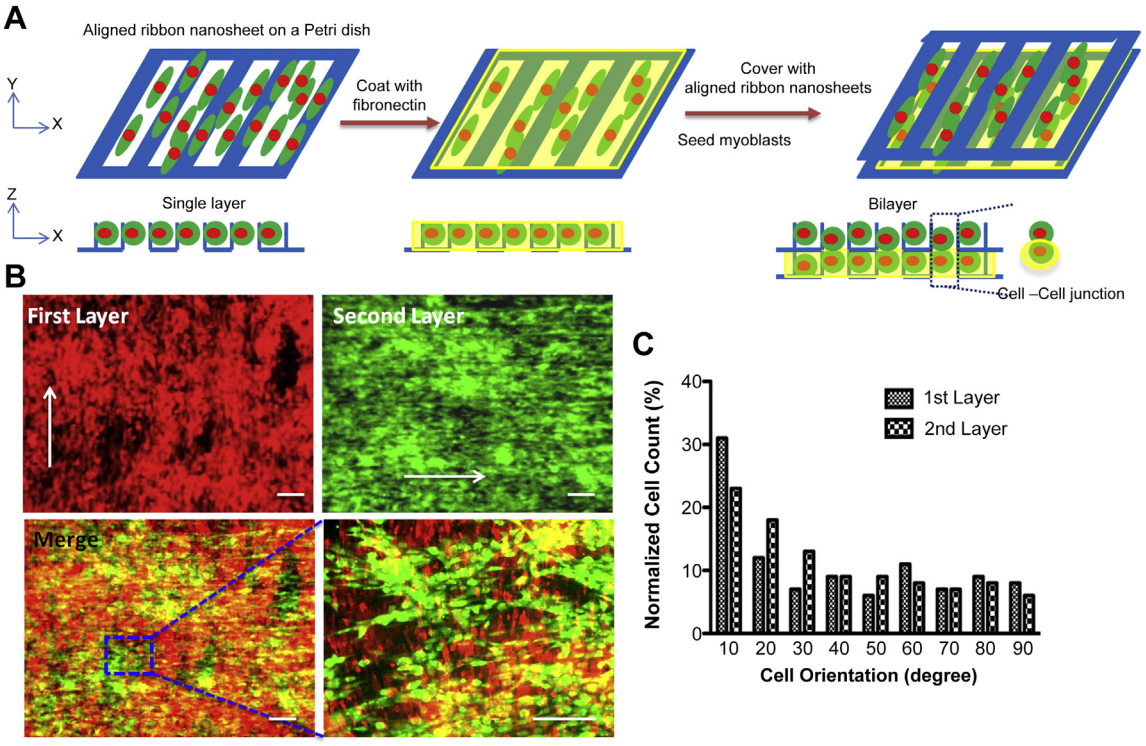


**Fig. 5.** Generation of bilayer C2C12 cell sheets at 8 days in cell culture media. (A) Schematics of the process of generating bilayer cell sheets with nanoribbon sheets. (B) Fluorescence images of cells on an anisotropic C2C12 cell layer. The cells on the first and second layers were stained using CellTracker Orange and Green, respectively (scale bars: 50 μm). (C) Histogram of cell orientation on the first and second layers. (For interpretation of the references to color in this figure legend, the reader is referred to the web version of this article.)

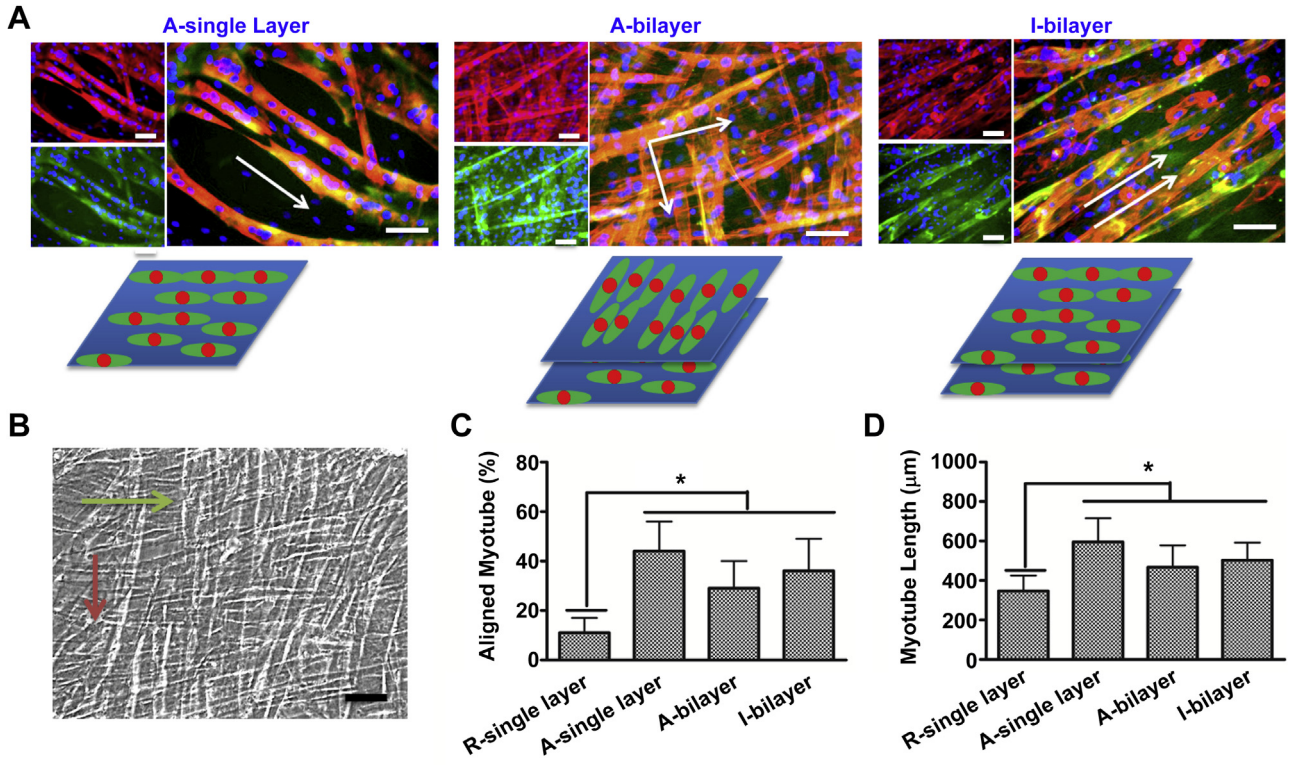


**Fig. 6.** Myotube formation on bilayer cell sheets at 12 days in cell differentiation media. (A) Immunofluorescence images of myotubes (green), F-actin (red), and nuclei (blue) from an anisotropic single layer (A-single layer), an anisotropic bilayer (A-bilayer, orthogonal) and an isotropic bilayer (I-bilayer, parallel) (scale bars: 100 μm). (B) Optical image of myotubes on an anisotropic bilayer (A-bilayer) (scale bar: 200 μm). (C) & (D) Orientation and length of myotubes on a random single layer (R-single layer, without nanoribbons), an anisotropic single layer (A-single layer), an anisotropic bilayer (A-bilayer) and an isotropic bilayer (I-bilayer). *Indicates statistical significance at the 95% confidence level compared with myotubes on an R-single layer. (For interpretation of the references to color in this figure legend, the reader is referred to the web version of this article.)

particular, the elasticity and surface topography of the C2C12 cell sheets were measured using a nanomechanical mapping technique [30–34]. As shown in Fig. 7, the Young's modulus of the cell sheet was (2.97 ± 0.46) kPa, which is close to that of natural muscles (24–115 kPa) [34]. In contrast, the Young's modulus of the control (Petri dish), (6.63 ± 1.14) MPa (in hydrated condition), was significantly higher than that of the cell sheets and natural muscles. Thus, we confirmed that the mechanical property of the cell sheets was similar to those of natural muscles.

Supplementary video related to this article can be found at http://dx.doi.org/10.1016/j.biomaterials.2015.02.028.

### 3.6. Gene expression of C2C12 cells on the bilayer cell sheets

To further confirm the induced myogenic commitment of the C2C12 myoblasts cultured on the oriented bilayer cell sheets, quantitative reverse transcription-polymerase chain reaction (qRT-PCR) was performed. Fig. 8 illustrates the expression levels of myogenic genes in the cells in the random (R-bilayer), anisotropic (A-bilayer, orthogonal) and isotropic (I-bilayer, parallel) bilayer cell sheets, compared with random (R-single layer) and anisotropic (A-single layer) single-layer cell sheets. To compare the gene expression levels between the cells in the bilayer and single-layer culture systems, we designed a control construct (referred to as a mixed single layer) that was produced from two separated single-layer cell sheets with the same cell density and culture periods (12 days for first layer and 5 days for second layer) as those of the bilayer cell sheets. The cells on the aligned bilayer cell sheets exhibited the upregulation of myogenin (an essential factor that is required for the fusion of myoblasts into myotubes, the development of myogenesis, and the repair of skeletal muscles) and Myf-6 (also referred to as MRF4 and associated with the fusion of myoblasts into myotubes), with levels ~2.0- and ~3.9-fold higher, respectively, than the expression levels in the random bilayer cell sheet and ~5.0- and ~15.0-fold higher, respectively, than the expression levels in the control construct [35]. MHCIIa and MHCIId(x), which are genes related to the myosin heavy chain (MHC, the motor protein of filaments in the muscle that has a central role in muscle contraction), exhibited higher expression levels in the bilayer cell sheets compared with the levels in the single layer [36].

## 4. Discussion

It is well known that cellular microenvironments appear to play a central role in cell specification. In fact, cells sense and feel the elasticity of the local matrix environment, and transducers relay various physical and biological signals among cells, including signals associated with protein expression, morphological changes, and lineage specification [30,37]. Therefore, a bottom up strategy to recapitulate the complex structures of extracellular matrix in native tissues is attractive from practical and scientific perspectives [38–40]. For example, Engler et al. created poly(acrylamide) based synthetic matrices with different mechanical properties to direct the differentiation of stem cells into specific lineages when cultured on a matrix with similar physical properties to those of the tissue or organ of interest [30]. In fact, when myoblasts were cultured on a fully rigid dish or on a flask composed of polystyrene, the contraction effort was isometric. In contrast, on a compliant matrix, such as a collagen hydrogel or myoblastic cell sheets, the myoblasts were able to contract [41].

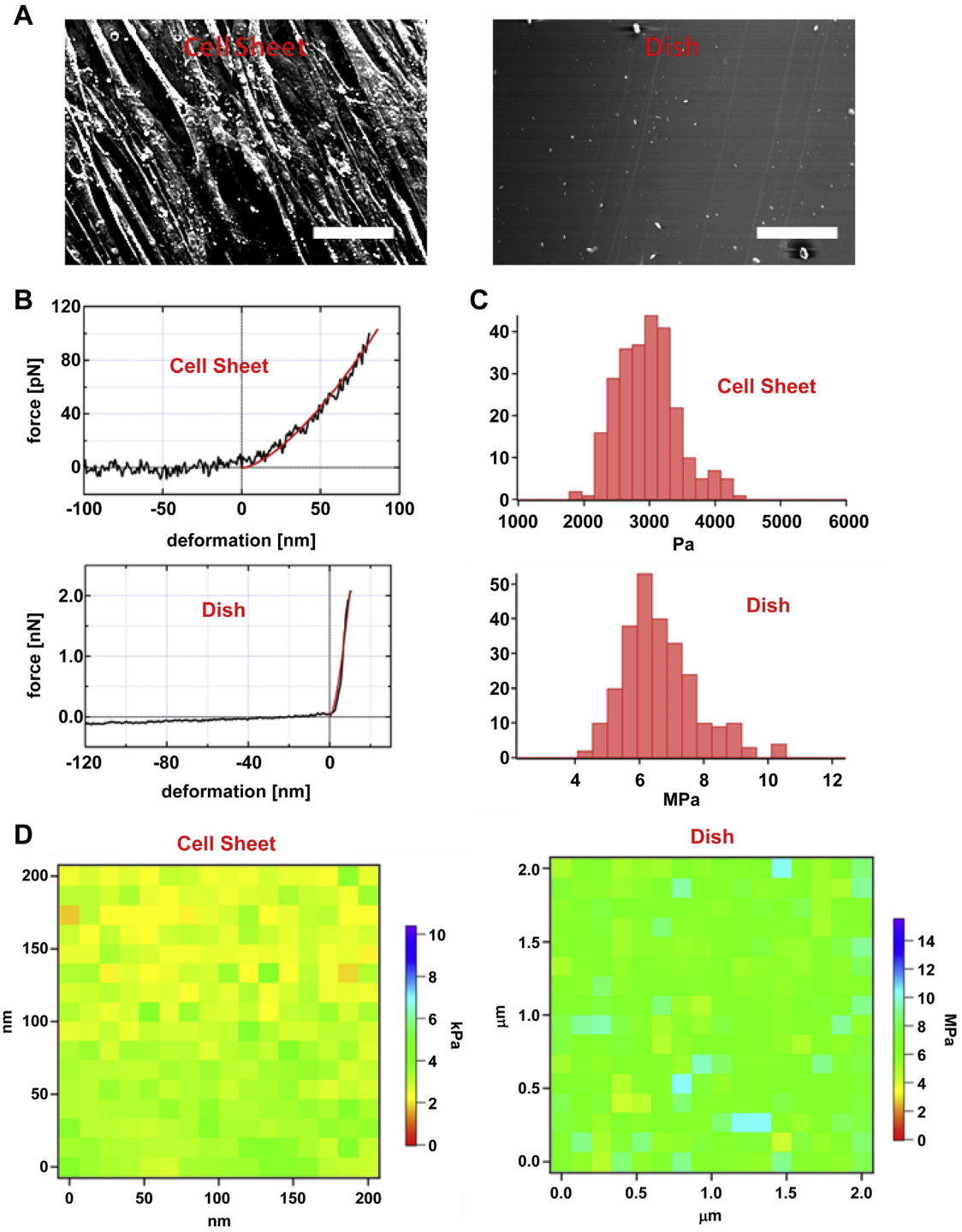


**Fig. 7.** (A) Morphology, (B) force deformation curves, (C) histograms in Young's modulus, and (D) nanomechanical mapping of a single-layer C2C12 cell sheet (at 8 days) and control (Petri dish).

In this regard, we expect that the mature myoblastic cells in the first layer not only served as a biomimetic matrix, but also might have released certain myogenic signal molecules to catalyze the myogenesis of the cells in the second layer. Therefore, constructing multilayer cell sheets using the nanoribbon sheets would be one of successful paradigms of solving directed-assembly of cells. Indeed, due to the exquisite microscale and nanoscale architecture, ECM directs various cell behaviors, including alterations in cell adhesion, morphology, orientation, and various intracellular signaling pathways, exquisitely harnessing cell behaviors such as cell orientation in different layers would be a great challenge. Thus, the developed nanoribbon sheets displayed great potential in building multilayer oriented cell sheets.

Furthermore, the advantage of these PLGA nanoribbon sheets for constructing organized cell layer is attributed to their unique microscopic morphology. The aligned nanoribbons were connected to the strips on each of their sides, which enhances their organization and alignment. When constructing multilayer cell sheets, the slots between two adjacent ribbons facilitate the cell–cell interaction in different layers [42,43]. Besides, the canal-

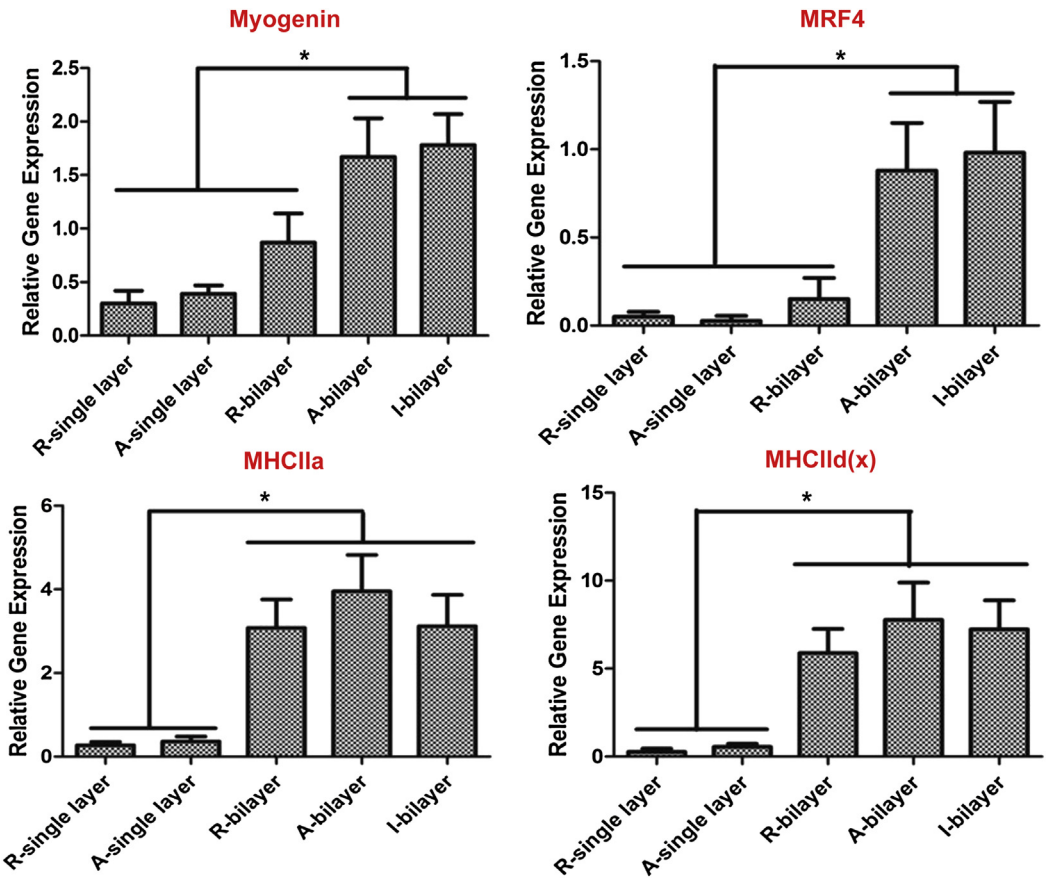


**Fig. 8.** Gene expression in C2C12 cells (at 12 days) cultured on a random single layer (R-single layer, without nanoribbons), an anisotropic single layer (A-single layer), a random bilayer (R-bilayer), an anisotropic bilayer (A-bilayer, orthogonal) and isotropic bilayer (I-bilayer, parallel). *Indicates statistical significance at the 95% confidence level. The housekeeping gene β-actin was used as an internal control to normalize the gene expression levels.

like structure of nanoribbons allows efficient cell seeding, as previously described [44]. When cells were seeded on conventional grooved micropatterns, most of the cells resided in the grooved regions. However, in the canal-like micropatterns, cells resided both in the canal-like ribbons and in the slots between each aligned ribbons at high densities (Fig. S3). Therefore, the nanoribbons are suitable for the assembly of various on-demand structures with isotropic or anisotropic alignment.

The bilayer cell sheets demonstrated in this work will be useful to create a physiological milieu to catalyze myogenesis [18,45–47]. In fact, the nanoribbon sheet served as an engineered scaffold which directed the cellular organization with high cell density and good alignment in short seeding days due to their unique microstructure. Such precisely and rapidly patterning technique is essential for enhancing minimally invasive delivery of cellular constructs in cell transplantation. In addition, the nanoribbon sheet may allow for the construction of hierarchical cellular constructs by multilayering each cell layer, that is also useful for the generation of thick muscle tissues with densely packed cells (e.g. skeletal muscle, cardiac tissue) in the application of bioactuators and drug screening devices [48–50].

## 5. Conclusion

We developed freestanding PLGA nanoribbon sheets, which supported cell anchorage, orientation, and proliferation in 2D and 3D cellular organizations. The nanoribbons allowed for the alignment of C2C12 cells into bilayer cell sheets, and the cell alignment was easily controlled by regulating the direction of the nanoribbons. Moreover, bilayer cell sheets with anisotropic (orthogonal) and isotropic (parallel) orientations were successfully engineered. The bilayer sheets of aligned C2C12 cells effectively promoted cell differentiation into mature myotubes. Additionally, the cell alignment enhanced the expression of myogenic genes. We believe that directing cell bilayer or multilayer assembly using nanoribbons could facilitate the engineering of synthetic tissues for regenerative medicine and drug-screening applications.

## Acknowledgments

This work was supported by the World Premier International Research Center Initiative (WPI) and JSPS KAKENHI: Grant Number 25870050 (T. F.) from MEXT, Japan, and Mizuho Foundation for the Promotion of Sciences (T. F.). H. K. W. acknowledges the support of the Hong Kong RGC (GRF 604712 and GRF 605210).

## Appendix A. Supplementary data

Supplementary data related to this article can be found at http://dx.doi.org/10.1016/j.biomaterials.2015.02.028.

## References

[1] Khademhosseini A, Langer R, Borenstein J, Vacanti JP. Microscale technologies for tissue engineering and biology. Proc Natl Acad Sci U S A 2006;103:2480–7.
[2] Zorlutuna P, Annabi N, Camci-Unal G, Nikkhah M, Cha JM, Nichol JW, et al. Patterning of functional neovessels using a 'living' microvascular stamp. Adv Mater 2012;24:1782–804.

[3] Ross AM, Jiang Z, Bastmeyer M, Lahann J. Physical aspects of cell culture substrates: topography, roughness, and elasticity. Small 2012;8:336–55.
[4] Waterston RH, Thomson JN, Brenner S. Mutants with altered muscle structure in *Caenorhabditis elegans*. Dev Biol 1980;77:271–302.
[5] Aubin H, Nichol JE, Hutson CB, Bae H, Sieminski AL, Cropek DM, et al. Directed 3D cell alignment and elongation in microengineered hydrogels. Biomaterials 2010;31:6941–51.
[6] Albrecht DR, Underhill GH, Wassermann TB, Sah RL, Bhatia SN. Probing the role of multicellular organization in three-dimensional microenvironment. Nat Methods 2006;3:369–75.
[7] Nahmias Y, Odde DJ. Micropattening of living cells by laser-guided direct writing: application to fabrication of hepatic-endothelial sinusoid-like structure. Nat Protoc 2006;1:2288–96.
[8] Mironov V, Boland T, Trusk T, Forgacs G, Markwald RR. Organ printing: computer-aided jet-based 3D tissue engineering. Trends Biotechnol 2003;21:157–61.
[9] Shi XT, Zhou J, Zhao Y, Li L, Wu HK. Gradient-regulated hydrogel for interface tissue engineering: steering simultaneous osteo/chondrogenesis of stem cells on a chip. Adv Healthc Mater 2013;2:846–53.
[10] Shi XT, Zhao Y, Zhou J, Chen S, Wu HK. One-step generation of engineered drug-laden poly(lactic-co-glycolic acid) micropatterned with Teflon chips for potential application in tendon restoration. ACS Appl Mater Inter 2013;5:10583–90.
[11] Shi XT, Chen S, Zhou J, Yu H, Li L, Wu HK. Directing osteogenesis of stem cells with drug-laden, polymer-microsphere-based micropatterns generated by Teflon microfluidic chips. Adv Funct Mater 2012;22:3799–807.
[12] Hosseini V, Ahadian S, Ostrovidov S, Camci-Unal G, Chen S, Kaji H, et al. Engineered contractile skeletal muscle tissue on a microgrooved methacrylated gelatin substrate. Tissue Eng A 2012;18:2453–65.
[13] Fujie T, Matsutani N, Kinoshita M, Okamura Y, Saito A, Takeoka S. Adhesive, flexible, and robust polysaccharide nanosheets integrated for tissue-defect repair. Adv Funct Mater 2009;19:2560–8.
[14] Fujie T, Okamura Y, Takeoka S. Ubiquitous transference of a free-standing polysaccharide nanosheet with the development of a nano-adhesive plaster. Adv Mater 2007;19:3549–53.
[15] Fujie T, Mori Y, Ito S, Nishizawa M, Bae H, Nagai N, et al. Micropatterned polymeric nanosheets for local delivery of an engineered epithelial monolayer. Adv Mater 2014;26:1699–705.
[16] Okamura Y, Kabata K, Kinoshita M, Miyazaki H, Saito A, Fujie T, et al. Fragmentation of poly(lactic acid) nanosheets and patchwork treatment for burn wounds. Adv Mater 2013;25:545–51.
[17] Jiang C, Tsukruk VV. Freestanding nanostructures via layer-by-layer assembly. Adv Mater 2006;18:829–40.
[18] Yamato M, Okano T. Cell sheet engineering. Mater Today 2004;7:42–7.
[19] Shi XT, Wang Y, Varshney RR, Ren L, Zhang F, Wang DA. In-vitro osteogenesis of synovium stem cells induced by controlled release of bisphosphate additives from microspherical mesoporous silica composite. Biomaterials 2009;30:3996–4005.
[20] Shi XT, Wang Y, Ren L, Gong Y, Wang DA. Enhancing alendronate release from a novel PLGA/hydroxyapatite microspheric system for bone repairing applications. Pharm Res 2009;26:422–30.
[21] Zolnik BS, Burgess DJ. Effect of acidic pH of PLGA microsphere degradation and release. J Control Res 2007;122:338–44.
[22] Fujie T, Ahadian S, Liu H, Chang H, Ostrovidov S, Wu H, et al. Engineered nanomembranes for directing cellular organization toward flexible biodevices. Nano Lett 2013;13:3185–92.
[23] Tay CY, Irvine SA, Boey FYC, Tan LP, Venkatraman S. Micro-/nano-engineered cellular responses for soft tissue engineering and biomedical applications. Small 2011;7:1361–78.
[24] Kolewe ME, Park H, Gray C, Ye X, Langer R, Freed LE. 3D structural patterns in scalable, elastomeric scaffolds guide engineered tissue architecture. Adv Mater 2013;25:4459–65.
[25] Ostrovidov S, Shi X, Zhang L, Liang X, Kim SB, Fujie T, et al. Biomaterials 2014;35:6268–77.
[26] Huang NF, Patel S, Thakar RG, Wu J, Hsiao BS, Chu B, et al. Myotube assembly on nanofibrous and micropatterned polymers. Nano Lett 2006;6:537–42.
[27] Okazaki K, Holtzer H. Myogenesis: fusion, myosin synthesis, and the mitotic cycle. Proc Natl Acad Sci U S A 1966;56:1484–90.
[28] Li Z, Paulin D. Different factors interact with myoblast-specific and myotubes-specific enhancer regions of the human desmin gene. J Biol Chem 1993;268:10403–15.
[29] Engler AJ, Griffin MA, Sen S, Bönnemann CG, Sweeney HL, Discher DE. Myotubes differentiate optimally on substrates with tissue-like stiffness: pathological implications for soft or stiff microenvironments. J Cell Biol 2004;166:877–87.
[30] Engler AJ, Sen S, Sweeney HL, Discher DE. Matrix elasticity directs stem cell lineage specification. Cell 2006;126:677–89.
[31] Stevens MM, George JH. Exploring and engineering the cell surface interface. Science 2005;310:1135–8.
[32] Nakajima K. Polymer physics from suspensions to nano-composites and beyond. Hoboken: NJ: John Wiley & Sons; 2010. p. 129 [Chapter 3].
[33] Liu H, Fujinami S, Wang D, Nakajima K, Nishi T. Nanomechanical mapping on the deformed poly (ε-caprolactone). Macromolecules 2011;44:1779–82.
[34] Mathur AB, Collinsworth AM, Resichert WM, Kraus WE, Truskey GA. Endothelial, cardiac muscle and skeletal muscle exhibit different viscous and elastic properties as determined by atomic force microscopy. J Biomech 2001;34:1545–53.
[35] Jennings CGB. Expression of the myogenic gene MRF4 during Xenopus development. Dev Biol 1992;150:121–32.
[36] Arber S, Halder G, Caroni P. Muscle LIM protein, a novel essential regulator of myogenesis, promotes myogenic differentiation. Cell 1994;79:221–31.
[37] Shi X, Chen S, Zhao Y, Lai C, Wu H. Enhanced osteogenesis by a biomimic pseudo-periosteum-involved tissue engineering strategy. Adv Healthc Mater 2013;2:1229–35.
[38] Nichol JW, Khademhosseini A. Modular tissue engineering: engineering biological tissues from the bottom up. Soft Matter 2009;5:1312–9.
[39] Elbert DL. Bottom-up tissue engineering. Curr Opin Biotechnol 2011;22:674–80.
[40] Khademhosseini A, Langer R. Microengineered hydrogels for tissue engineering. Biomaterials 2007;28:5087–92.
[41] Al-Rekabi Z, Pelling AE. Cross talk between matrix elasticity and mechanical force regulates myoblast traction dynamics. Phys Biol 2013;10:066003.
[42] Nishiguchi A, Yoshida H, Matsusaki M, Akashi M. Rapid construction of three-dimensional multilayered tissues with endothelial tube networks by the cell-accumulation technique. Adv Mater 2011;23:3506–10.
[43] Harring H, Cato P, Salazar F, Wilkinson M, Knox A, Haycock JW, et al. Immunocompetent 3D model of human upper airway for disease modeling and in vitro drug evaluation. Mol Pharm 2014;11:2082–91.
[44] Shi XT, Fujie T, Saito A, Takeoka S, Hou Y, Shu Y, et al. Periosteum-mimetic structures made from freestanding microgrooved nanosheets. Adv Mater 2014;26:3290–6.
[45] Shimizu T, Yamato M, Kikuchi A, Okano T. Cell sheet engineering for myocardial tissue reconstruction. Biomaterials 2003;24:2309–16.
[46] Takahashi H, Shimizu T, Nakayama M, Yamato M, Okano T. The use of anisotropic cell sheets to control orientation during the self-organization of 3D muscle tissue. Biomaterials 2013;34:7372–80.
[47] Nagamori E, Ngo TX, Takezawa Y, Saito A, Sawa Y, Shimizu T, et al. Network formation through active migration of human vascular endothelial cells in a multilayered skeletal myoblast sheet. Biomaterials 2013;34:662–8.
[48] Levenberg S, Rouwkema J, Macdonald M, Garfein ES, Kohane DS, Darland DC, et al. Engineering vascularized skeletal muscle tissue. Nat Biotechnol 2005;23:879–84.
[49] Bach AD, Beier JP, Stern-Staeter J, Horch RE. Skeletal muscle tissue engineering. J Cell Mol Med 2004;8:413–22.
[50] Ostrovidov S, Hosseini V, Ahadian S, Fujie T, Prakash Parthiban S, Ramalingam M, et al. Tissue Eng Part B Rev 2014;20:403–36.